The glass transition in polymer melts - results from neutron scattering

1996 J. Phys.: Condens. Matter 8 9177

(http://iopscience.iop.org/0953-8984/8/47/007)

J. Phys.: Condens. Matter **8** (1996) 9177–9190. Printed in the UK

The glass transition in polymer melts—results from neutron scattering

D Richter

Institut für Festkörperforschung, Forschungszentrum Jülich, 52425 Jülich, Germany

Received 15 July 1996, in final form 27 August 1996

Abstract. The polymer dynamics near the glass transition can be classified into three different categories: (i) anomalous low-frequency vibrations, the so-called boson peak, which are accompanied by a fast relaxational process; (ii) secondary and higher-order relaxations, which are assumed to involve only local molecular motions and (iii) the structural relaxation underlying the flow processes which freezes at the glass transition. This paper presents inelastic and quasielastic neutron scattering data on these dynamical processes, emphasizing polybutadiene. In the light of these data, current models on the dynamic glass transition are inspected. In a second step, recent experiments on the coherent dynamic structure factor are exploited in order to learn about the molecular nature of the various polymer motions.

1. Introduction

Glass formation and the glass transition are very general phenomena taking place in a large variety of different materials encompassing the traditional silicate glasses, molecular and ionic liquids, metglasses, polymers and even biological macromolecules [1–3]. Similar to phase transitions, despite the large breath of materials, rather universal phenomena are associated with the glass process. Very general are multiple relaxation processes with stretched exponential relaxation functions and time scales deviating substantially from an Arrhenius temperature behaviour. In addition anomalous low-frequency vibrations—the so-called boson peak—and fast relaxation-like excitations appear to be general [4, 5]. Furthermore, a number of low-temperature features such as tunnelling states or specific heat and heat conduction anomalies are found in many materials [6]. This similarity of phenomena suggests underlying general principles which are a present focus of research in condensed matter physics.

This paper selects polymers as an example to test ideas on the vibrational and relaxational dynamics of disordered materials in the neighbourhood of the glass transition T_g [7–19]. Polymers have particular advantages for the investigation of glass transition phenomena: (i) due to their irregular microstructure crystallization can be avoided in general; (ii) changing from protonated to deuterated materials, the coherent and incoherent scattering may be studied easily, thereby highlighting the pair or selfcorrelation functions respectively.

The paper is organized as follows. First we briefly review pertinent phenomena relating to the glass transition in polymers. Thereafter, in the light of these results current models are inspected and finally we report on the exploitation of the coherent dynamic structure factor, in order to learn about the space–time development of molecular motions.

0953-8984/96/479177+14$19.50

2. Pertinent experimental results

The dynamics of the glass process is characterized by an enormous range of time scales requiring in general the application of a variety of different experimental methods in order to access the different motions. Figure 1 displays a relaxation map for (1–4) polybutadiene (PB), sketching the major dynamical features of a glass forming polymer. The data points shown are taken from dielectric studies [20], from measurements of the dynamical modulus [21] and from neutron scattering [5, 7, 9]. We distinguish three different dynamical regimes. (i) The freezing process is controlled by the structural α-relaxation exhibiting a pronounced non-Arrhenius temperature dependence, which phenomenologically is well described by a Vogel–Fulcher temperature dependence: $\tau^{-1} \propto \exp(-B/(T - T_0))$. (ii) At a temperature about 20% above T_g a secondary relaxation process, the β_{slow} relaxation, splits from the α-process. Other than the primary α-relaxation β_{slow} follows an Arrhenius law and is not affected by the glass transition. (iii) At high frequencies, in the picosecond range, the boson peak and the associated fast relaxation process called β_{fast} are indicated. Following figure 1 the relevant time scales for the glass process from the boson peak and the fast relaxations to the freezing α-relaxation span 14–15 orders of magnitude.

The frequency regime in the range of the boson peak and the β_{fast} process is documented by figure 2 [22]. There, coherent inelastic spectra from 1–4 PB are shown after scaling with the Bose occupation factor and the Debye–Waller factor. For a perfect harmonic solid such a scaling should reveal the same spectrum for all temperatures. The data show that this is indeed the case for frequencies above about 3 meV and below T_g roughly for all frequencies. The data show that the boson peak at about 2 meV remains unchanged below the glass transition temperature. Towards higher $T > T_g$ at low frequencies additional intensity develops, indicating the onset of relaxation and/or significant vibrational softening of the material. We further note that at high frequencies in the 'harmonic regime' $S(Q, \omega) \propto g(\omega)/\omega^2 \propto 1/\omega$, indicating a density of state $g(\omega) \propto \omega$, which is characteristic for a dynamical matrix with random elements [23].

Features of the low-frequency dynamics in PB as seen by neutron spin echo spectroscopy (NSE) are displayed in figure 3, showing the intermediate dynamic structure factor $S(Q, t)/S(Q, 0)$ of PB measured close to the first minimum of the static structure factor $S(Q)$ [9]. According to the time–temperature superposition principle the time dependence of $S(Q, t)$ was rescaled with the time scale of the α-relaxation as obtained from dynamic mechanical measurements [24]. Above the merging temperature of α and β_{slow} relaxation $T_m = 220$ K (see figure 1) the different spectra collapse to a single master curve following a Kohlrausch–William–Watts (KWW) time dependence: $\tau_{KWW}^{-1} \approx \exp\left(-(t/\tau_0)^{\beta}\right)$ with $\beta = 0.41$. Below 220 K severe deviations from scaling are observed, which are accompanied by an increase of the amplitude of the relaxation function. As we shall see this deviation from scaling is a signature of the β_{slow} process. Finally we note that as a consequence of the fast dynamical processes, which are outside the observation window of NSE, the normalized scattering function in figure 3 does not approach unity at short times.

3. Inspection of current models

Dynamic features of the glass transition have recently been discussed in terms of several theories and models [3, 11, 25, 26]. The most celebrated among them, the mode coupling theory (MCT), has been compared thoroughly with the neutron scattering results from PB [22, 27]. A detailed repetition would surpass the space limitations of this article. Here we only wish to outline some of the main results of this comparison and concentrate on two

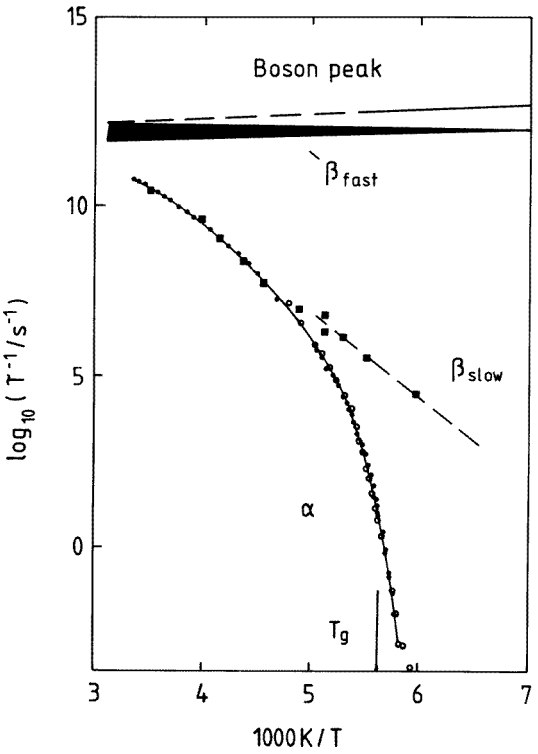

Figure 1. A relaxation map for (1–4) polybutadiene covering the prevailing dynamical features around the glass transition. The frequency ranges for the boson peak and the associated fast relaxation-like dynamics (β_{fast}) are indicated schematically. The full and open circles along the α-relaxation trace represent dielectric [20] and mechanical [21] results respectively. The full squares display characteristic rates obtained from neutron spin echo spectroscopy [7, 9]. The time scale of the α-process has been shifted to match that of the microscopic data. The dashed line represents the temperature dependence of the β_{slow} process observed by dielectric spectroscopy [17].

less well known approaches: the coupling model of Ngai *et al* [25, 26] and its application by Colmenero *et al* [14], and the vibration relaxation model of Buchenau *et al* [11, 10].

3.1. The MCT

Qualitatively the MCT is able to reproduce the prevailing experimental features observed in PB quite well. (i) The two-step nature of the relaxation process above the α–β_{slow} merging temperature T_m; (ii) the apparent existence of a characteristic temperature T_c which coincides with T_m and (iii) the predicted anomalies in the temperature dependence of the amplitude $f(Q) \propto (T_c - T)^{1/2}$ for the slow relaxational process as well as the temperature law for the minimal susceptibility $\chi''_{\min} \propto (T - T_c)^{1/2}$ are experimentally verified. On the other hand (iv) the divergences in the time scales at T_c do not occur; (v) the predicted relationship between the critical exponents cannot be verified for PB and finally (vi) the β_{slow} relaxation, though an inherent phenomenon of the glass process, is not predicted in the MCT. Whether extended versions of the MCT [3] would be able to quantitatively account for the experimental results has not yet been investigated.

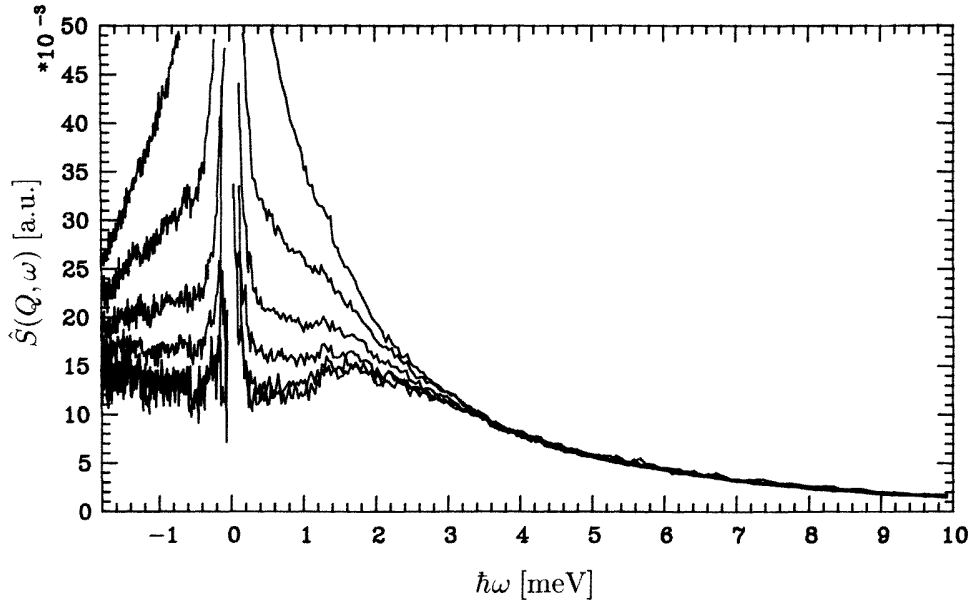

Figure 2. The dynamic structure factor $S(Q,\omega)$ from polybutadiene at $Q = 1.4$ Å^{-1} at temperatures, from the top, of 240, 200, 180, 160, 120 and 100 K. The presented spectra are obtained by subtracting the elastic line and scaling with the Bose and Debye–Waller factors [22].

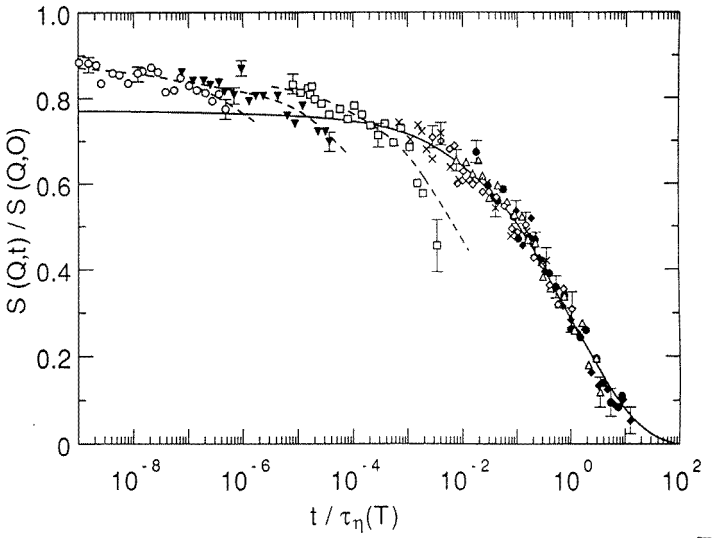

Figure 3. Selected NSE spectra obtained at $Q = 1.88$ Å^{-1} from PB [9]. The time has been rescaled to the microscopic viscosity scale. (♦, 280 K; ●, 260 K; △, 250 K; ◊, 240 K; +, 230 K; □, 205 K; ▼, 190 K; ○, 180 K) The solid line represents the master curve obtained from the spectra at temperatures higher than 220 K. The dashed lines represent individual fits to the low-temperature data.

3.2. The coupling model

With the coupling model (CM) Ngai [25] postulates on phenomenological grounds the existence of two well separated time regimes in glassy relaxation. (i) The first is an

uncoupled microscopic regime where the relaxational process takes place not yet influenced by the presence of the other molecules. This regime is characterized by a microscopic time τ_0 and a crossover time t_c. For $t < t_c$ the relaxation is single exponential. (ii) For times longer than t_c in the macroscopic time regime coupling between the motions of different molecules takes place and the relaxation function $\Phi(t)$ changes to a stretched exponential governed by a macroscopic time τ^*. $\Phi(t)$ then has the form

$$\Phi(t) = \begin{cases} \exp(-t/\tau_0) & t < t_c \\ \exp(-(t/\tau^*)^\beta) & t > t_c. \end{cases} \tag{1}$$

Finally continuity at t_c requires

$$\tau^* = \left(t_c^{\beta-1}\tau_0\right)^{1/\beta}. \tag{2}$$

Recently, features of the coupling model were investigated on PB. A series of rheological studies on PB with different microstructures addressed the relation between fragility and stretching parameter implied by (2) [21]. Using polymers from the same family it is reasonable to assume that the microscopic times remain constant and are not influenced by the microstructure. Then (2) suggests that increasing stretching is connected to an increased fragility. Qualitatively, this behaviour was found. Going from (1–4) to (1–2) PB the β-value in the rheological experiment drops from 0.49 to 0.41. At the same time the temperature dependence of the α-process becomes steeper, indicating an increasing fragility.

Macroscopic experiments such as measurements of the dynamic modulus or the viscosity only access the macroscopic time while inelastic neutron scattering also addresses the microscopic relaxation processes. Recently, Zorn *et al* [13] evaluated neutron spectra from PB in the spirit of the CM: inelastic neutron spectra are due to vibrations and relaxations. In order to remove the vibrational part, an *ansatz* of Colmenero *et al* [14] was used, which describes the incoherent intermediate scattering function in terms of a product of a vibrational $S_{vib}(Q, t)$ and a relaxational part $S_{rel}(Q, t)$. As a first approximation, assuming harmonic phonons, the vibrational part was extrapolated from low-temperature data, revealing the relaxational scattering function $S_{rel}(Q, t) = S(Q, t)/S_{vib}(Q, t)$. Figure 4 displays relaxational scattering functions thus determined for PB at $Q = 1.4$ Å^{-1} for several temperatures. Their shape suggests an interpretation in terms of Ngai's model. After about 1.5 ps an initial single exponential decay crosses over to a stretched exponential relaxation. Thereby, the crossover time appears not to depend either on temperature or on Q. Colmenero *et al* [14] associate the initial Debye process with conformational dynamics not yet hindered by the presence of other chains. This interpretation is supported by the activation energies found for the initial process, which for a number of polymers agrees well with rotational barriers [13].

3.3. The vibration relaxation model

The vibration relaxation model (VRM) [11, 13] origins from the soft-potential model used for a description of the disordered solid. The amorphous material is treated like a large molecule, where at least for the low-lying excitations the dynamical matrix is assumed to have random elements. Wigner [23] has shown that the density of eigenvalues of such a random matrix lies within a Wigner circle around the origin of eigenvalue space. Close to the eigenvalue $\lambda = 0$ the density of states is constant with equal probability for positive and negative eigenvalues. Negative eigenvalues give rise to double-minimum potentials separating two stable states by a low barrier. The VRM connects vibrations within the shallow potentials with low-barrier relaxations in the double-minimum potentials

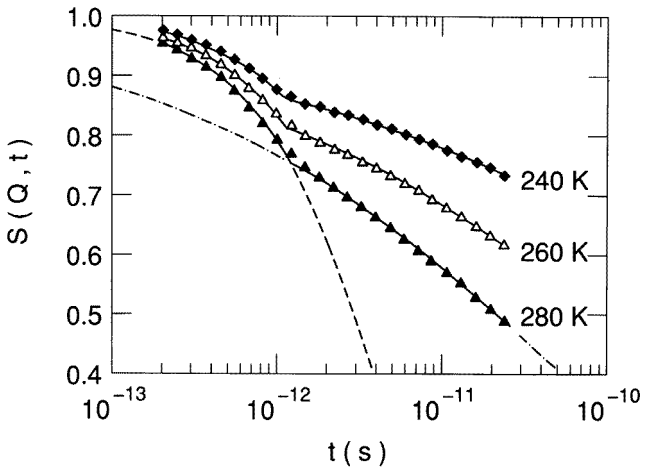

Figure 4. The relaxational part of the intermediate scattering function of PB for $Q = 1.4$ Å^{-1}. The dashed and dashed–dotted lines show fits of the fast regime to a Debye relaxation and the slow regime to a Kohlrausch relaxation function respectively [13].

and describes both relaxational processes and vibrational processes within the same set of potentials. The relaxational dynamics is taken in Kramer's [28] weak-coupling limit relating the phonon damping γ to the transition rates Γ across the barriers

$$\Gamma = \gamma(E_A/kT)\exp(-E_A/kT). \tag{3}$$

E_A thereby is the barrier height in the double-minimum potential. From the constant eigenvalue density $S(Q,\omega) \propto 1/\omega$ follows naturally. In order to describe the boson peak, an empirical expression is used which for low and high frequencies assumes the correct sound wave and Wigner mode density limits. Thereby, an additional parameter, the boson peak frequency ω_B, is introduced. The detailed calculations of $S(Q, t)$ are lengthy and therefore not repeated here [13]. Figure 5 displays fits of the VRM to inelastic spectra from PB without deconvoluting the vibrational scattering function as done in figure 4. The quality of the fit shows that the inelastic spectra can be well expressed in terms of this model. We note that taking the total inelastic spectra including the vibrations no indication for a discontinuous change in the scattering function (see figure 4) can be seen. Deviations occurring at long times and higher temperatures most likely relate to flow processes which are not incorporated in the VRM.

The model parameters obtained in the fitting procedures follow the expected temperature dependences. The Wigner frequency ω_0 reflecting the slow degrees of freedom is essentially independent of temperature. The Debye frequency ω_D determining the scattering in the sound wave limit $\omega \to 0$ agrees well with the corresponding Brillouin sound velocities. Astonishing and unexpected is the very strong anharmonicity of the boson peak frequency ω_B, which in the VRM denotes the crossover between sound waves and random matrix description. The high anharmonicity of the boson peak modes would correspond to a Grüneisen parameter of the order of 15 compared to 5.5 for the sound waves—a result which is difficult to understand. While in the case of PB it may be argued that this extreme result is model dependent—at high temperatures a clear boson peak cannot be distinguished—also for polyisobutylene, where the boson peak persists to nearly 100 K above T_g, similar strong shifts are found [15]. Finally, the phonon damping parameter

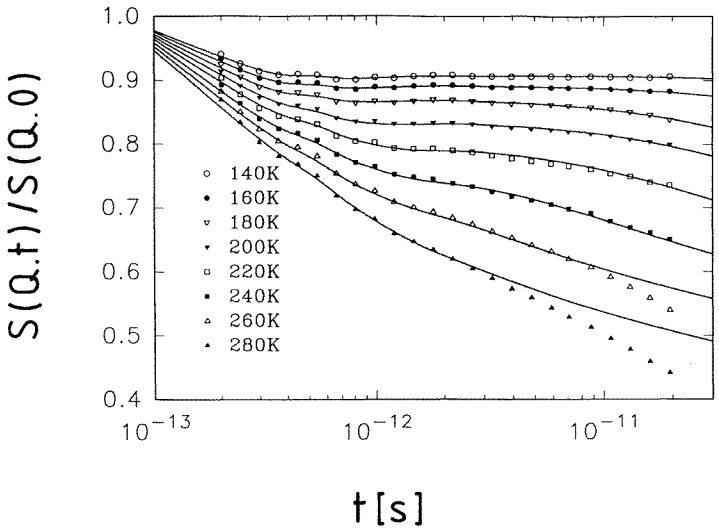

Figure 5. The full intermediate scattering function of PB for $Q = 1.4$ Å^{-1}. The continuous lines show fits to the VRM.

γ, also determining the relaxation rates (3) can be well related to third-order anharmonic interactions yielding $\gamma(T) \propto \langle u^2 \rangle^2 / T$ where $\langle u \rangle^2$ is the mean square atomic displacement obtained from Debye–Waller factor measurements.

Summarizing, the VRM describes successfully incoherent neutron scattering spectra in the range of the picosecond dynamics up to temperatures of 50 K above T_g. For higher temperatures and longer times, deviations occur which are due to the negligence of flow processes. This outcome is complementary to what was found earlier for the MCT approach, where the main deviations occurred below the critical temperature $T_c \approx 214\ \mathrm{K} = T_g + 37\ \mathrm{K}$. The performance of both theories can be understood from their origins. While the VRM starts from the amorphous solid being an extension of the tunnelling and the soft-potential model, the MCT originates from the liquid state extending to the highly supercooled situation.

4. Coherent dynamic structure factors

Though the relaxation dynamics of polymers and other glass forming materials has been investigated by relaxational methods for at least five decades, still little is known about the underlying molecular motions. In principle, varying the momentum transfer Q, quasielastic and inelastic neutron scattering is capable of providing the space–time resolution in order to access the relaxations and vibrations on a molecular level. In this section we present first results on the coherent form factor associated with the fast process [19] and discuss coherent quasielastic data on the relaxational dynamics in the α–β_{slow} merging region [17, 18].

Following the mode coupling implication of a decoupling of Q and ω dependences in the dynamic structure factor previous investigation concentrated on the frequency behaviour as discussed above. We now want to focus on the Q-dependence of the coherent inelastic scattering. Figure 6(a) shows the Q-dependence of the inelastic scattering from PB for two different frequencies, one near to the elastic window and the other one at a slightly

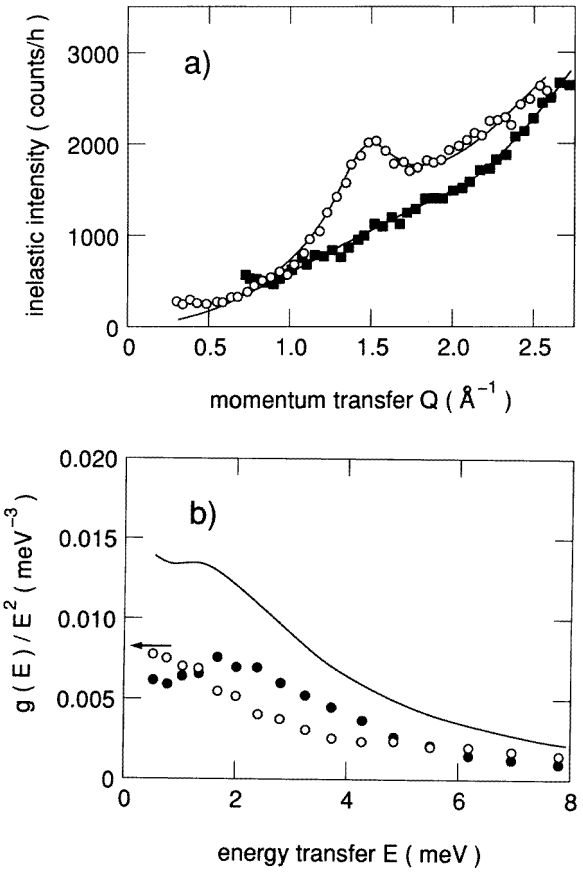

Figure 6. (*a*) The Q-dependence of the inelastic scattering from PB at two different frequencies (○ , 0.7 meV, ■, 5 meV) at 207 K together with the fits described in the text. (*b*) Results from an analysis of the dynamic structure factor interms of sound waves and additional excitations as a function of energy transfer. The effective densities of states are plotted in the form of density of state divided by frequency squared. Full line, total density of states; ○ , sound wave contributions; ● , additional excitations; arrow, limit for the sound wave density of states from Brillouin scattering [19].

higher frequency around 5 meV, at 207 K, about 30 K above T_g. Immediately it is clear that the decoupling approximation is not valid. While the Q-dependence near the elastic line reproduces the static structure factor peak at 1.5 Å^{-1}, the one at higher frequency does not. This holds for the whole temperature range between 60 and 300 K. Without any further analysis the data in figure 6(a) demonstrate the presence of two different kinds of low-frequency dynamics. The first relates to a correlated motion of neighbouring polymer chains and dominates at low frequencies. The other corresponds to uncorrelated motion, prevailing at frequencies above the boson peak (2 meV).

The idea of two different types of low-frequency motion, sound waves and local excitations, is well established in the frame of low-temperature properties of amorphous solids [6], where low-temperature anomalies are traced to interactions between sound waves and local excitations. Figure 6(a) suggests a similar picture for undercooled liquids: correlated motion of chains, e.g. sound waves, coexist with local excitations,

one dominating at lower and the other at higher frequencies. In this spirit the data were fitted by a superposition of a sound wave dynamic structure factor following essentially a $Q^2 S(Q, \omega = 0)$ law [29] and a form factor for additional excitations being close to a simple $Q^2 \exp(-\langle u^2 \rangle Q^2)$ behaviour. Figure 6(b) displays the result of this analysis at the glass transition temperature T_g. The following results pertain. (i) The total density of states agrees within experimental error with that determined from incoherent spectra of equivalent protonated PB. (ii) This density of states is decomposed into a sound wave and an additional part. The sound wave part thereby contributes significantly at low frequencies and decreases substantially above the boson peak at 2 meV, where the density of states from the additional excitation undergoes a maximum. (iii) The sound wave part thereby looks like a broad quasielastic line and does in fact account for a large part of the intensity attributed to the famous fast picosecond process. (iv) Finally, the sound wave part extrapolates accurately to the Debye density of states calculated from acoustic and Brillouin data for longitudinal and transversal waves.

Using the inelastic coherent form factors as a fingerprint, a sizeable part of the low-frequency dynamic structure factor can be associated with correlated in-phase molecular motions. The correlation range ξ of this collective motion may be estimated from the width in Q of the sound wave form factor $\xi = 2\pi/\Delta Q \approx 15$ Å. Superimposed is a vibrational pattern whose form factor does not deviate significantly from the conventional incoherent phonon form factor within the Q-range of the measurements. These results show experimentally the essential role of long-range correlated motion in the low-frequency dynamics of glasses and undercooled liquids and raises questions on the models discussed in section 3. (i) If there existed a β_{fast}-relaxation regime of the mode coupling type, the investigated frequencies, which encompass the fast quasielastic component (figure 6(b)) could not lie in this MCT regime. If they did they should exhibit the same Q-dependence. (ii) An interpretation of the fast process in terms of local conformational dynamics yet unaffected by neighbouring chains assumed in the frame of the CM will have to be revised, in order to include the nonlocal character of the fast dynamics. (iii) Finally also the vibrational relaxation model assuming overbarrier jumps for possibly extended normal modes will have to explicitly incorporate collective fast motions.

We now turn to the α and β_{slow} relaxations in PB and inspect the dynamic structure factor at the position of the first and second peaks of $S(Q)$—the first peak or amorphous halo thereby relates mainly to interchain correlations while the second peak originates from interchain distances [30]. Figure 7 displays NSE spectra taken at both peak positions. The data were rescaled with the time scale τ_η set by the viscosity relaxation. While at the first peak all data collapse onto a single master curve which can be described by a stretched exponential using the dielectric stretching exponent $\beta_{diel} = 0.41$, at the second peak the spectra do not follow the time–temperature superposition principle determined by τ_η and strong deviations from a single master curve are obvious.

Extracting characteristic times from both sets of spectra those from the interchain peak follow, as already signified by the master plot, the Vogel–Fulcher temperature dependence of the α relaxation, while those from the second peak obey an Arrhenius law with an activation energy identical to that of the dielectric β relaxation [17]. Thus, at the two first structure factor peaks essentially different aspects of the chain dynamics are observed; at the interchain peak the diffusive structural relaxation stands out, while at the intrachain peak the more local β_{slow} relaxation dominates the density fluctuations.

In the range of pure β_{slow} relaxation below the merging temperature T_m the main features of the dynamic structure factor can be understood in terms of a simple model based on local jump processes with jump rates determined by a Gaussian distribution of energy barriers as

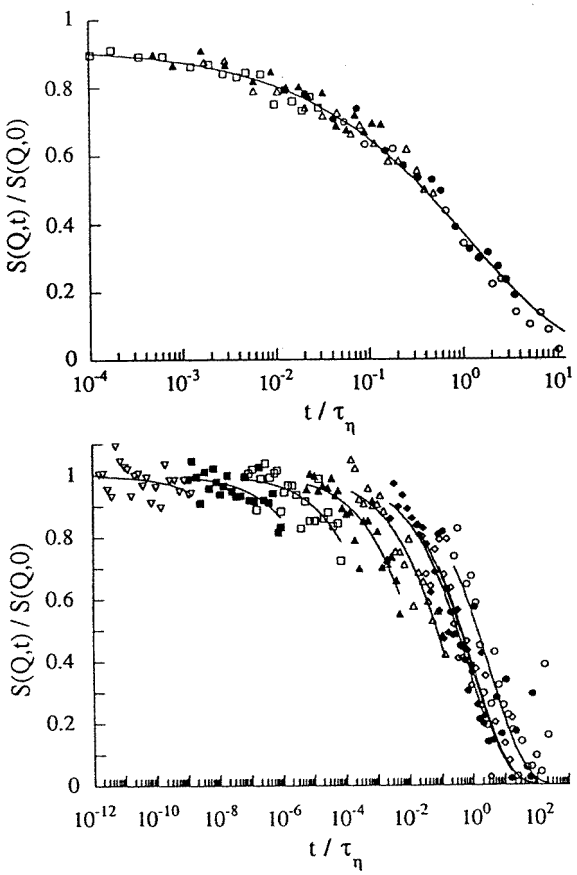

Figure 7. A scaling representation of NSE data from PB at $Q = 1.48$ Å^{-1} (○ , 280 K; ● , 260 K; △, 240 K; ▲, 230 K; □, 220 K (upper figure)) and at 2.71 Å^{-1} (○ , 300 K; ● , 280 K; ◇, 260 K; ◆, 240 K; △, 220 K; ▲, 205 K; □, 190 K; ● , 180 K; ▽, 170 K (lower panel). The solid lines correspond to KWW functions (see the text) [18].

derived from dielectric relaxation. The β_{slow} relaxation is assumed to be a spatially localized process. The simplest picture of an elemental motion is a jump of an atom between two equivalent sites separated by a distance d with a characteristic time $\tau = \tau_0 \exp(E_A/kT)$. For such hopping processes the incoherent intermediate scattering function is given by

$$S_{inc}^{hop}(Q,\, t) = 1 - \frac{1}{2}\left(1 - \frac{\sin Qd}{Qd}\right) + \frac{1}{2}\left(1 - \frac{\sin Qd}{Qd}\right) \mathrm{e}^{-2t/\tau}$$
$$= 1 - A^{hop}(Q,\, d) + f^{hop}(Q,\, d,\, \tau,\, t). \tag{4}$$

Coherent and incoherent scattering differ with respect to the presence of interference terms in the coherent scattering. Let us consider the jump motion of a pair of atoms. If such atomic jumps are uncorrelated, dynamic constructive interferences are absent and it follows naturally that the dynamic quasielastic part assumes the form of the incoherent part. Note, however, that interference terms from the average atom distribution remain, giving rise to $S(Q)$. If the motions are correlated it can be shown that interference effects are small as long as the jump distances are smaller than the distances between atom pairs. Under this

assumption the coherent inelastic part can be approximated by the incoherent inelastic part and the normalized coherent scattering function can be written as

$$(S_{coh}(Q,\,t))/(S(Q)) = 1 - (A^{hop}(Q,\,d))/(S(Q)) + (f^{hop}(Q,\,d,\,\tau,\,t))/(S(Q)). \tag{5}$$

The secondary relaxation cannot be described by means of a single Debye process; more

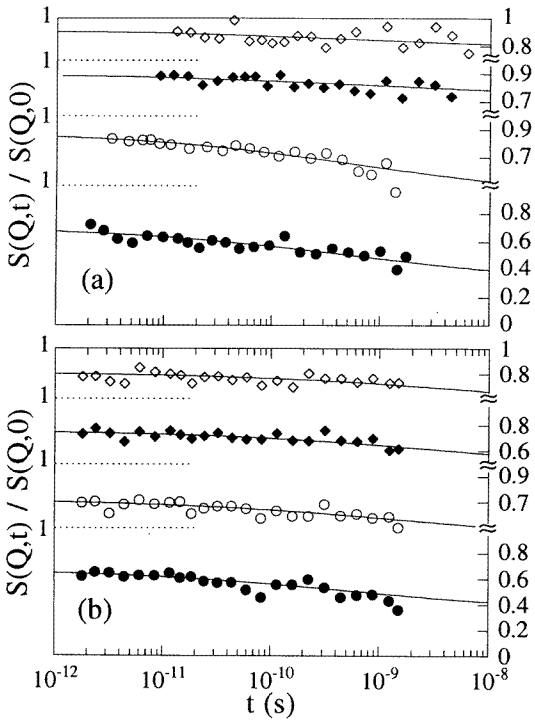

Figure 8. NSE spectra from PB. (*a*) at $T = 205$ K and for different Q-values (◇, 1.4 Å^{-1}, ♦, 1.56 Å^{-1}, ○ , 1.88 Å^{-1}, ● , 2.55 Å^{-1}) and (*b*) at $Q = 2.71$ Å^{-1} and for various temperatures (◇, 170 K; ♦, 180 K; ○ , 190 K; ● , 205 K). The ordinates corresponding to each spectrum are given on the left- and right-hand sides respectively. Solid lines correspond to the fit with the hopping model for the β-relaxation [17].

complicated relaxation functions involving distributions of relaxation times, such as the Cole–Cole function or distributions of energy barriers, such as log-normal functions [31], have to be used for its description. For PB the dielectric β-relaxation function can be well described by assuming a superposition of Debye elemental processes with a Gaussian distribution of energy barriers $g(E)$ [17],

$$\varphi_\beta(t) = \int_0^\infty g(E) \exp\left[\frac{-t}{\tau_0^D \exp(E/kT)}\right] \mathrm{d}E \tag{6a}$$

$$g(E) = \left(1/\sqrt{\pi}\sigma\right) \exp\left[-\left((E - E_0)/\sigma\right)^2\right]. \tag{6b}$$

Here σ is the width and E_0 is the average of the distribution of activation energies. The width σ decreases linearly with temperature ($\sigma\,(\mathrm{eV}) = 0.145\text{–}2.55 \times 10^{-4} T$ (K)). This narrowing of the relaxation function with increasing temperature is another well established feature of the β-relaxation [31]. The values of τ_0^D and E_0 are determined from the temperature dependence of the position of the maximum of the relaxation, $\tau_{\max} = \tau_0^D \exp(E_0/kT)$ and

they are $\tau_0^D = 3.5 \times 10^{-17}$ s and $E_0 = 0.41$ eV. The coherent dynamic structure factor corresponding to the β-process can now be built by a superposition of the coherent scattering functions for the elemental processes (5) weighted by the Gaussian distribution function of the activation energies $g(E)$

$$\frac{S(Q,t)}{S(Q)} = 1 - \frac{1}{S(Q)} \int_0^\infty g(E) A^{hop}(Q, d(E))\, \mathrm{d}E + \frac{1}{S(Q)} \int_0^\infty g(E) f^{hop}(Q, d(E),\ \tau(E), t)\, \mathrm{d}E. \tag{7}$$

The free parameters in this model are τ_0^{NSE}, the prefactor in the Arrhenius law for the elemental jumps and the jump distance d. Figure 8 displays the result of the fit with this model to the Q- and T-dependent spectra. Implying for the jump distance the slight barrier energy dependence of the soft-potential model $d \propto E_A^{1/4}$ a most probable jump distance of $d = 1.5$ Å evolves. Furthermore, the experiment reveals the very astonishing result that the density fluctuations which are directly observed by the neutrons decay two orders of magnitude faster than the dipole reorientations seen by dielectric spectroscopy ($\tau_0^{NSE} > \tau_0^D/250$).

Figure 9 displays the relative quasielastic contribution of the β_{slow} process to the structure factor as calculated on the basis of the parameters obtained by the fitting procedure.

$$F(Q) = \frac{1}{S(Q)} \int_0^\infty g(E) f^{hop}(Q,\ d(E), \tau(E), t)\,|_{t=0}\, \mathrm{d}E\ . \tag{8}$$

The result explains immediately the qualitatively different behaviour of $S(Q, t)$ at the

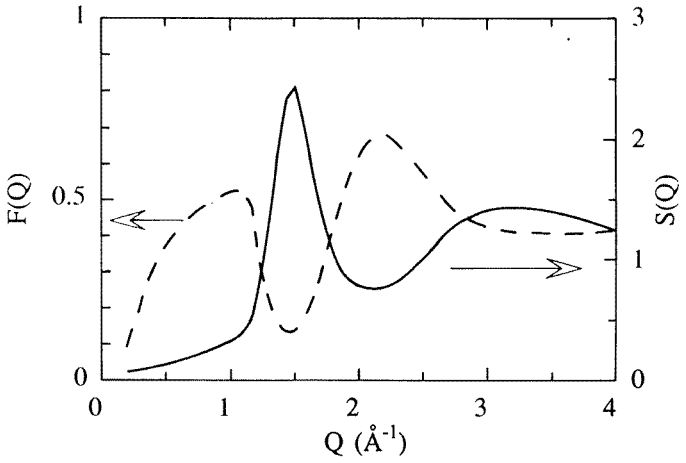

Figure 9. The amplitude $F(Q)$ of the relative quasielastic contribution of the β_{slow} process to the coherent scattering function obtained from the hopping model as a function of Q. The static structure factor $S(Q)$ at 160 K is shown for comparison (solid line) [17].

first two maxima of $S(Q)$. Due to the renormalization of the quasielastic part in (4) with $S(Q)$ the contribution of the β_{slow} process at the first maximum of $S(Q)$ is minute, while it becomes very strong close to the second maximum, explaining the Arrhenius behaviour of the characteristic times at high Q. Further evaluation considering explicitly the coherent form factor of the moving rigid building blocks of the chain (*cis*- and *trans*-units involving the double bond) essentially confirms the outcome of the analysis within the simple hopping

model [18]. For an interpretation of the scattering data at higher temperatures in the merging regime of α and β_{slow} relaxations we refer to [18].

5. Conclusions

This paper presented recent neutron scattering results on the dynamic glass transition in polymers emphasizing PB. Particular attention was placed on measurements of the Q- and ω- or t-dependent dynamic structure factor. Around the glass transition temperature dynamic phenomena take place over a wide range in time. On the high-frequency end anomalous vibrations—the boson peak—and associated with them fast relaxation-like motions—the β_{fast} process—take place. A study of the coherent dynamic structure factor in this regime shows that an important part of this fast dynamics is collective in nature, displaying sound wave-like characteristics.

Measurements of the dynamic structure factor in the range of the primary (α) and secondary (β_{slow}) relaxations showed the following. (i) The temperature dependence of the α time scale is universal—all methods from NSE (microscopic) up to rheology (macroscopic) reveal the same dynamics; i.e. at the level of the interchain distances the relaxations follow the same time law as the macroscopic flow. (ii) The dynamic structure factor also led to some insight into the nature of the secondary β_{slow} relaxation, identifying it as an intrachain relaxation process with elementary jumps of an average jump distance of 1.5 Å.

Relating the neutron data to current models we showed that the vibration relaxation and the MCT offer interpretations of the experiments on complementary time scales. Originating from the soft-potential model the VRM describes properties of undercooled polymer liquids from the perspective of the amorphous solid. The modelling of the fast relaxation in terms of jumps in double-minimum potentials breaks down when the lifetime of these potentials reaches the characteristic times for overbarrier jumps. On the other hand the MCT starts with microscopic equations for the dynamics of liquids and is able to reproduce the initial states of undercooling. As soon as solid-like hopping processes come into play, which are dealt with in more advanced versions of MCT, the theory loses a lot of its appeal. The transition range between the more solid-like behaviour, where VRM is appropriate, and the more liquid-like properties, which are the region of MCT, coincides with the merging regime of the α and β_{slow} relaxations, which presently is not accounted for in any of these models. This temperature regime may hold the key for a general understanding of the glass process. Now it has become a focus of attention in experimental studies.

Acknowledgments

The author would like to thank many colleagues who helped to shape the experimental picture of the glass transition in polymers presented here. In particular U Buchenau, R Zorn, A Arbe and L Willner from Jülich, J Colmenero from San Sebastian and B Farago from Grenoble are gratefully acknowledged.

References

[1] Richter D, Dianoux A J, Petry W and Teixeira J (eds) 1989 *Dynamics of Disordered Materials (Springer Proceedings in Physics 37)* (Berlin: Springer)

[2] A J Dianoux, W Petry and D Richter (eds) *Dynamics of Disordered Materials II* 1993 (Amsterdam: North Holland)

[3] Goetze W 1991 *Liquids, Freezing and the Glass Transition* ed J P Hansen, D Levesque and J Zinn-Justin (Amsterdam: North Holland)
[4] Fujara F and Petry W 1987 *Europhys. Lett.* **4** 921
[5] Frick B, Richter D, Petry W and Buchenau U 1988 *Z. Phys.* B **70** 73
[6] W A Phillips (ed) 1981 *Amorphous Solids: Low Temperature Properties* (Berlin: Springer)
[7] Richter D, Frick B and Farago B 1988 *Phys. Rev. Lett.* **61** 2465
[8] Frick B, Farago B and Richter D 1990 *Phys. Rev. Lett.* **64** 2921
[9] Richter D, Zorn R, Farago B, Frick B and Fetters L J 1992 *Phys. Rev. Lett.* **68** 71
[10] Buchenau U 1992 *Phil. Mag.* B **65** 303
[11] Buchenau U, Schönfeld C, Richter D, Kanaya T, Kaji K and Wehrmann R 1994 *Phys. Rev. Lett.* **73** 2344
[12] Frick B and Richter D 1995 *Science* **267** 1939
[13] Zorn R, Arbe A, Colmenero J, Frick B and Buchenau U 1995 *Phys. Rev.* E **52** 782
[14] Colmenero J, Arbe A and Alegria A 1993 *Phys. Rev. Lett.* **71** 2603
[15] Frick B and Richter D 1993 *Phys. Rev.* B **47** 14 795
[16] Colmenero J, Alegria A, Alberdi J M, Alvarez F and Frick B 1991 *Phys. Rev.* B **44** 7321
[17] Arbe A, Buchenau U, Willner L, Richter D, Farago B and Colmenero J 1996 *Phys. Rev. Lett.* **76** 1872
[18] Arbe A, Richter D, Colmenero J and Farago B 1996 *Phys. Rev.* E at press
[19] Buchenau U, Wischnewski A, Richter D and Frick B 1996 *Phys. Rev. Lett.* at press
[20] Zorn R, Mopsik F, McKenna G B and Willner L, unpublished
[21] Zorn R, McKenna G B, Willner L and Richter D 1995 *Macromolecules* **28** 8552
[22] Zorn R, Richter D, Frick B and Farago B 1993 *Physica* A **201** 52
[23] Wigner E P 1958 *Ann. Math.* **67** 325
[24] Berry G B and Fox T G 1968 *Adv. Polym. Sci.* **5** 261
[25] Ngai K L 1979 *Comments Solid State Phys.* **9** 128; for an updated review, see *Disordered Effects on Relaxation Processes* 1994 ed R Richert and A Blumen (Berlin: Springer)
[26] Ngai K L, Arbe A and Colmenero J 1994 *Proc. Conf. on Quasielastic Neutron Scattering (San Sebastian, 1993)* ed J Colmenero, A Alegria, and J Bermejo (Singapore: World Scientific) p 277
[27] Richter D, Zorn R, Frick B and Farago B 1991 *Ber. Bunsenges. Phys. Chem.* **95** 1111
[28] Kramer H A 1940 *Physica* **7** 284
[29] Carpenter J M and Pelizarri C A 1989 *Phys. Rev.* B **12** 2391
[30] Frick B, Richter D and Ritter Cl 1989 *Europhys. Lett.* **9** 557
[31] See e.g. Crum N G, Read B E and Williams G 1967 *Anelastic and Dielectric Effects in Polymer Solids* (London: Wiley)